Pergamon

Journal of Structural Geology, Vol. 17, No. 6, pp. 819 to 830, 1995

0191-8141/95 $9.50+0.00

0191-8141(94)00101-4

Shear strain analysis and periodicity within shear gradients of metagranite shear zones

GÉRARD DUTRUGE,* JEAN-PIERRE BURG† and JOHANN LAPIERRE*

Centre Géologique et Géophysique, Université Montpellier II, Place Bataillon 34095 Montpellier, France

and

JEAN-LOUIS VIGNERESSE

CREGU-B.P. 23, 53501 Vandoeuvre-Les-Nancy Cedex, France

(*Received* 3 *June* 1994; *accepted in revised form* 8 *September* 1994)

Abstract—The distribution of natural ductile strain is studied by mapping continuous shear strain gradients across shear zones with widths of the order of tens of centimetres. The shear zones are derived from granites and the most ductile mineral (quartz) accommodates most of the rock deformation. Shear strain maps are based on quartz grain orientation, and finite strain maps on the shape of quartz grains measured by image analysis. Shear strain distribution shows discrete bands parallel to the shear plane, which reflect the strain localization. Strain profiles across the strain maps are compared to exponentially decreasing profiles. The significant variations of shear strain after subtraction of the smoothed profile are checked by Fourier analysis in terms of wavelengths. With this information at hand, we argue that shear strain distribution in shear gradients is periodic.

INTRODUCTION

Deformation of the continental crust is often concentrated in shear zones with thickness ranging from millimetres to several kilometres (Bak *et al.*, 1975) and these are often composed of an anastomosing network subparallel to the shear boundary. Geologists have investigated individual shear zone geometries in order to estimate the relative displacement involved (e.g. Ramsay & Graham 1970) and to comprehend tectonic implications for deep deformation of the lithosphere. Shear zones are characterized by a sigmoidal schistosity (e.g. Ramsay & Graham 1970, Ramsay & Allison 1979). Strain profiles published in the literature have been constructed from displacement and reorientation of passive markers (Ramsay 1980) such as surface traces of axes of anticlines (Weijermars 1987), dykes (Escher *et al.* 1975) and crystalline aggregates (Burg & Laurent 1978). Some field workers have described minor shear zones parallel to the boundary of kilometres-wide thrust-sense shear zones (e.g. Grocott & Watterson 1980). The amount of deformation, the width and the density of the minor shear zones increases concurrently toward the central part of the large scale shear zone (Escher *et al.* 1975). Therefore, strain is localized at several scales in a rock volume. Due to the scarcity of markers and subsequent lack of coverage of measurements, high frequency variations are in practice smoothed and profiles are drawn as approximate exponential curves (Ramsay 1980, Rey 1992).

In this study, we assume that granitic rocks are polyphase aggregates and the rock strength is primarily governed by the volume fraction of the least competent phase (Burg & Wilson 1987, Tullis *et al.* 1991). Strain measurements are based on the orientation of schistosity (Ramsay & Graham 1970) and on the shape analysis of elliptical deformed particles and polycrystalline aggregates (Dunnet 1969). Image analysis is applied to isolate quartz grains in photographs of shear gradients. Strain is mapped on polished rock sections cut parallel to the lineation and perpendicular to the foliation (*XZ*-plane of the strain framework) to draw shear strain profiles at grain scale. Signal analysis techniques are applied to detect whether strain magnitudes are periodically distributed on the shear strain maps or the equivalent shear strain profiles.

IMAGE ANALYSIS

Sample description

Three shear zones resulting from a single ductile shear event are described in this paper (Fig. 1). They were chosen from different geological settings, so that strain partitioning features can be attributed to parameters independent of geological history.

Sample 1 (Fig. 1a) is a minor ductile shear zone related to a kilometre-wide, ductile transcurrent fault (La Marche fault) in the northern French Massif Central

*Present address: Laboratoire de Tectonophysique, Université Montpellier II, Place Bataillon, 34095 Montpellier, France.

†Present address: Geologisches Institut, ETH Zentrum, Sonneggstrasse 5, CH-8092 Zürich, Switzerland.

(Choukroune *et al.* 1983). The regional shearing episode was dated to 310 Ma (Choukroune *et al.* 1983) and the granite was dated between 315 and 325 Ma (Duthou *et al.* 1984). The protolith is a leucogranite with an average grain size of about 0.2 cm (for quartz, K-feldspar and plagioclase). The polished rock section is ca. 20 cm wide. A continuous gradient from extremely deformed to nearly unstrained granite is exposed. For the sake of simplification, we will use the term *mylonite* to describe the strongly foliated facies forming the intensely strained part of the shear gradients, where the foliation has been turned to parallel to the shear plane direction. Temperature of deformation was 400°C ± 50°C (Rey 1992) and the sample has experienced plane strain (shape of the strain ellipsoid, $K \approx 1$; Flinn 1962).

Sample 2 (Fig. 1b) comes also from the La Marche area. The mean grain size of the granite protolith is approximately 0.5 cm (for quartz, K-feldspar and plagioclase) and the rock section is nearly 40 cm wide from the mylonite to the granite. From petrological evidence (crystallization of muscovite at the expense of K-feldspar) and from microstructural measurements (quartz *c*-axis diagram showing prismatic <*a*> glide mechanism: Rey 1992), the temperature of deformation is estimated between 350 and 450°C. This sample has experienced plane strain.

Sample 3 (Fig. 1c), from the Pinet laccolith (Eastern Rouergue in the southern French Massif Central), has been fully described by Burg & Laurent (1978). *PT* conditions of deformation are $T \geqslant 350$°C and $P \geqslant 2.5$ kbar (Burg & Teyssier 1983). Strain analysis was done in *XZ* thin sections (i.e. the plane perpendicular to the foliation and parallel to the lineation), cut perpendicularly to the mylonite foliation. Grain size is about 0.15 cm in the less strained protolith. The continuous section studied, 15 cm wide, presents a gradient between high to low strained fabrics. Deformation is plane strain.

Strain markers

In the three samples, quartz is sufficiently abundant to build an almost regular and compact network (35 volume per cent; Fig. 2a) and provide a high density of measurements. The amount of polycrystalline quartz aggregates has no significant variation across the gradients, which suggests bulk isovolumetric deformation. Evidence suggests that quartz accommodates most strain of the rock by plastic deformation involving dynamic recrystallization. Although the change in shape and orientation depends on several factors, including the state of finite strain and the mechanism of deformation (Ramsay & Allison 1979), analysing quartz grain shape may still provide a means to estimate the minimum strain for small amounts of finite strain. Therefore, we use quartz to estimate strain in the shear gradients.

Automatic sample analysis

Samples have been sawn according to the structural measurements. The polished cross-section are perpendicular to the foliation plane and parallel to the lineation. These *XZ* sections are scanned in order to obtain 256-grey tone images. The resolution was taken as 200 dpi (dots per inch; 79 pixels cm^{-1}), and so, representative grains are represented by at least 10 pixels. Quartz aggregates (Fig. 2a) are identified by image analysis software as light-grey particles which we call grains. In order to analyze the shape of individual grains, grains still connected after automatic analysis were separated manually after referring to thin-section photographs. The shape analysis was performed on separated particles. The image was rendered binary and the grain shapes were quantified by fitting ellipses to the grain outlines. The ellipse axial ratio (R) and long axis orientation (θ) define the grain shape fabric. The mylonite direction equated with the *C*-plane direction is taken as the reference for the orientation θ, positive in a clockwise rotation. We will first present in detail the analysis carried out on sample 1 to test the validity of the method and results.

STRAIN DISTRIBUTION WITHIN THE MYLONITE GRADIENTS

Strain analysis methods

Shear strain has been estimated and checked, using four recognized techniques. The data acquisition process provides for each grain, both the ellipse axial ratio (R) and its long axis orientation (θ). They are transformed into the shear strain (γ) and the axial ratio of the strain ellipse. Strain values have been determined using the shape analysis of each quartz grain and using the autocorrelation technique performed on extracted images with a squared outline; those method are compared only on sample 1.

With those methods, we estimate only the penetrative, bulk deformation and therefore we have not accounted for strain accumulated in shear bands (Fig. 2b, *C*- and *C'*-planes of Berthé *et al.* 1979). Consequently, methods based only on the reorientation and ellipticity of strain markers underestimate the total strain.

θ-map (orientation of long axes of ellipses). Orientation measurements from grain to grain are interpolated to create a regular grid of data with a squared mesh of approximately 0.25 cm^2. The resulting map is interpreted as the shear strain distribution (Fig. 3a), shear strain values (γ, gamma) being calculated by the angular relationship $\gamma = 2/\tan(2\theta)$ (Ramsay & Graham 1970). Quartz grains are flattened parallel to the schistosity and angles θ between the shear direction and schistosity range from 40° in the less strained facies to 5° near the mylonite centre of sample 1. Weak shear strain appears localized in bands 2–3 cm wide parallel to the shear direction and, hence noticeably larger than the ca. 0.2 cm grain size. Major bands are situated at 1.8 cm (#1), 5.5 cm (#2), 12.3 cm (#3) and 19.3 cm (#4) from the

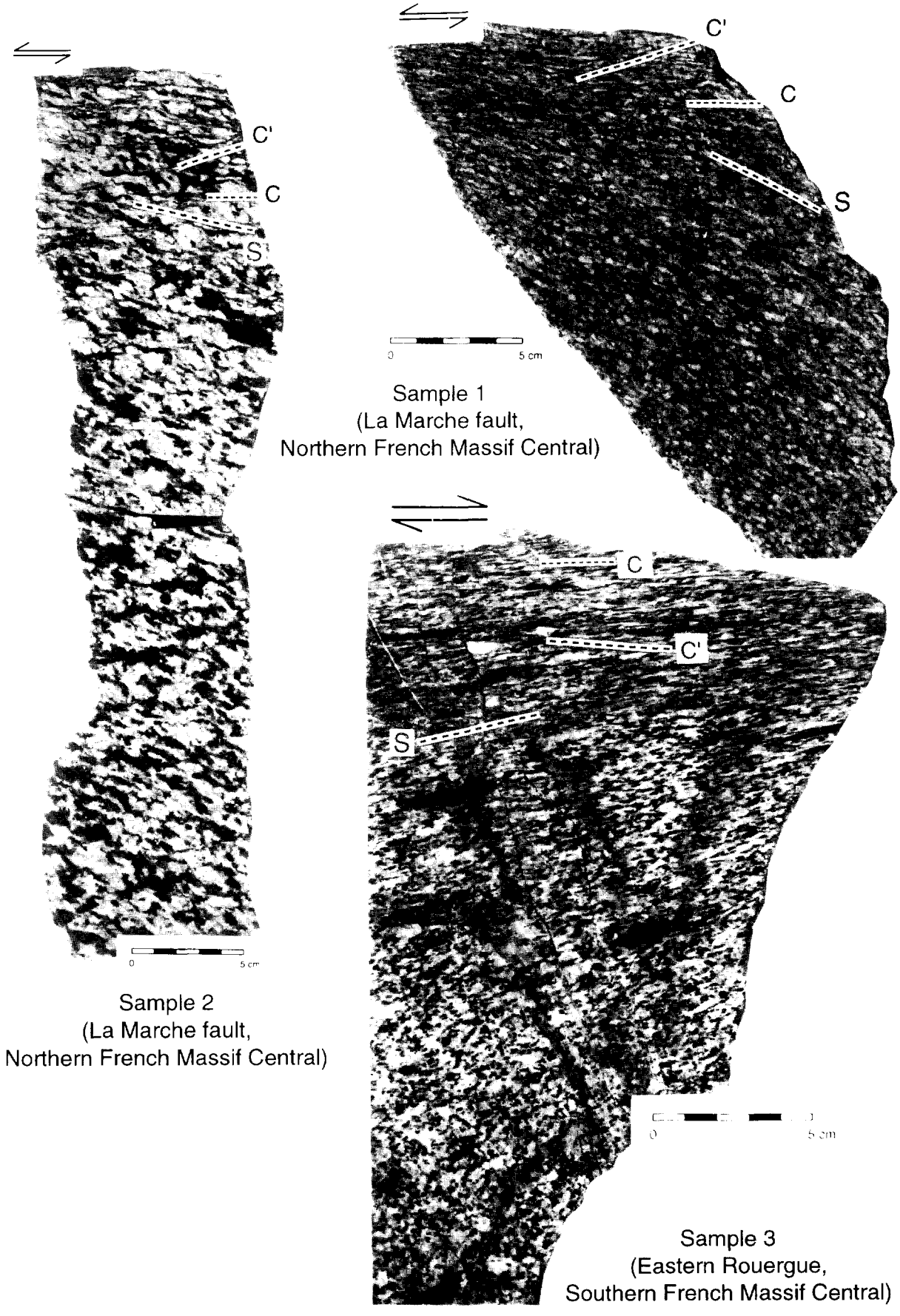

Fig. 1. Shear gradients in granitic rocks analysed in this paper. Schistosity (S) is defined by biotite in black and quartz in grey. C and C': shear planes (Berthe *et al.* 1979). In the highest strain zone (here called mylonite) S and C are parallel and are equated with the shear plane.

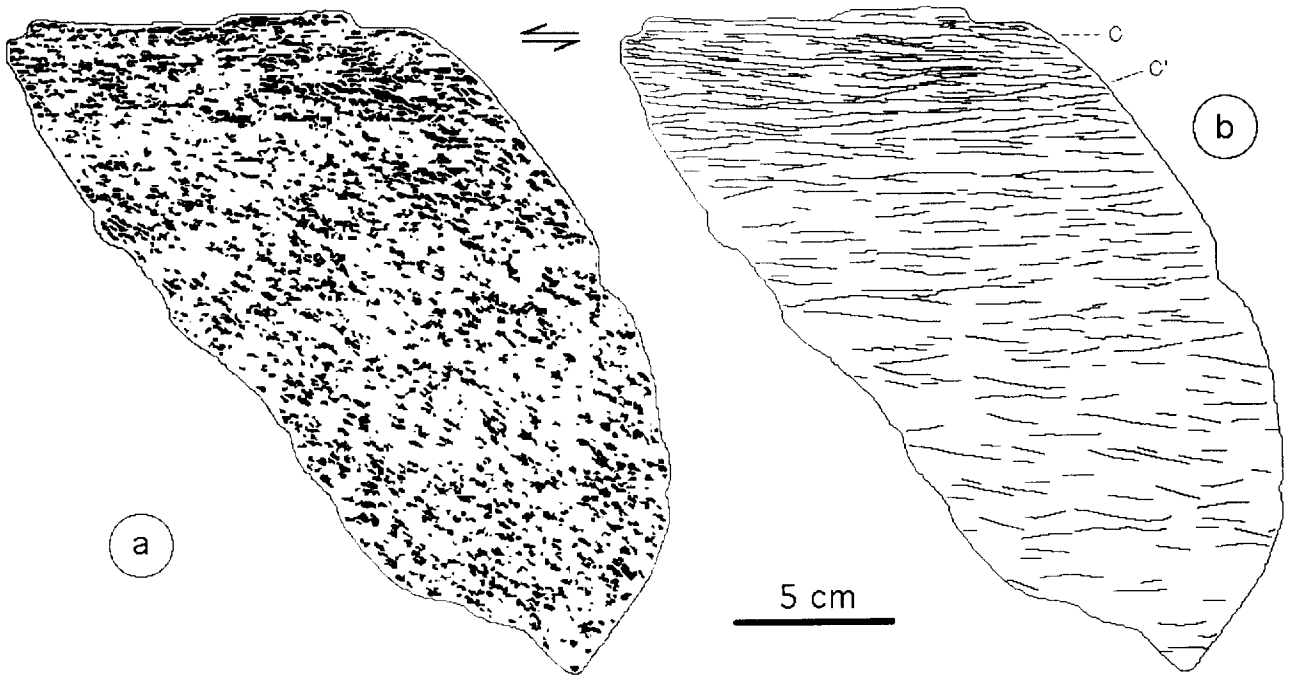

Fig. 2. Sample 1 petrostructural characteristics. (a) Quartz aggregates obtained by image analysis. Black regions denote quartz grains. (b) Shear planes defined by grain size reduction ($d \leq 50\ \mu m$) and a great concentration of phyllosilicates.

mylonite (Fig. 3a). Band (#1) is characterized by the strongest shear strain ($\gamma \geq 6$). Development and merging of shear planes in this band may induce localization on a continuous, fine grained (grain size $\leq 50\ \mu m$) network. The three other bands, with shear strain values around 4 (Fig. 3a) correspond to domains of low shear plane density (Fig. 2b).

R_f-*map* (*shape ratios*). The ellipticity of the strained quartz grains (shape ratio $R_m = X/Z$, X = long axis, Z = short axis, Ramsay & Huber 1983) yields the finite strain distribution. The same interpolation as above was applied to obtain a smoothed grid and a map (Fig. 3b). Finite strain variations fit the same four bands as those revealed on θ-maps (compare arrow labels 1, 2, 3 and 4 on Figs. 3a & b). There is a progressive increase of shape ratios in correlation with decreasing θ angles. From the comparison of the shear strain map (Fig. 3a) and the finite strain map (Fig. 3b), we can test whether strain is purely simple shear for each quartz grain. For perfect simple shear, the axial ratio of the strain markers are related to the orientation of the marker by: $R_c = (\text{cotan}(\theta))^2$ (Treagus 1981). The relative error ($(R_c - R_m)/R_m$) is, on average, 9.1% for the quartz grains of the sample 1. This error may be attributable to the influence of the non-simple shear rotation of the harder phases (K-feldspar, plagioclase and biotite) on the quartz grain shape. Therefore, we consider that more than 90% of quartz deformation is due to simple shear, and the shear strain analysis based on the simple-shear equation ($\gamma = 2/\tan(2\theta)$) is valid.

The autocorrelation function (*ACF*) (*Panozzo-Heilbronner* 1992). Generally, the autocorrelation is the measure of the similarity of a signal with itself when shifted along the sampling interval. Here, autocorrelation was applied to binary images of quartz grains to estimate strain components acting on the strain markers (quartz grains). Orientation (θ_s) and ellipse axial ratio (R_s) measured on the central part of the autocorrelation image are consistent with those obtained with the centre of gravity of the quartz grains, using the classical R_f–θ analysis (Lisle 1977) and the normalized centre-to-centre plots (Erslev 1988). Because of numerical constraint, the initial photograph is cut into squared images of 128 × 128 pixels (2.6 cm^2). The extracted images contain approximately 30 grains to define significant strain parameters. The images overlap by half their size vertically and laterally so that the measurement grid has a regular mesh of 0.8 cm. We obtained a map of shear strain (Fig. 3c) from the mean grain shape preferred orientation, θ_s, using the same equation as earlier ($\gamma = 2/\tan(2\theta_s)$), and a map yielding finite strain (Fig. 3d) from the R_s ellipticity of the average grain. The ACF maps of sample 1 (Figs. 3c & d) show again that strain is localized in almost the same bands, yet more discontinuous, than those revealed by the point-to-point analysis (Figs. 3a & b). Discontinuity in shear band localization may be related to the initially non-random distribution of quartz. Therefore, strain parameters estimated with a fixed size square measurement window do not have the same significance for different positions in the image.

The strain distribution analysis applied to quartz grains and ACF techniques yield essentially similar results and give a pattern of heterogeneous strain in bands nearly parallel to the shear direction. Therefore, these bands of strain localization are not method artefacts. The orientation of polycrystalline aggregates (i.e. schistosity) with respect to the shear direction provides the fastest and the most accurate technique for estimat-

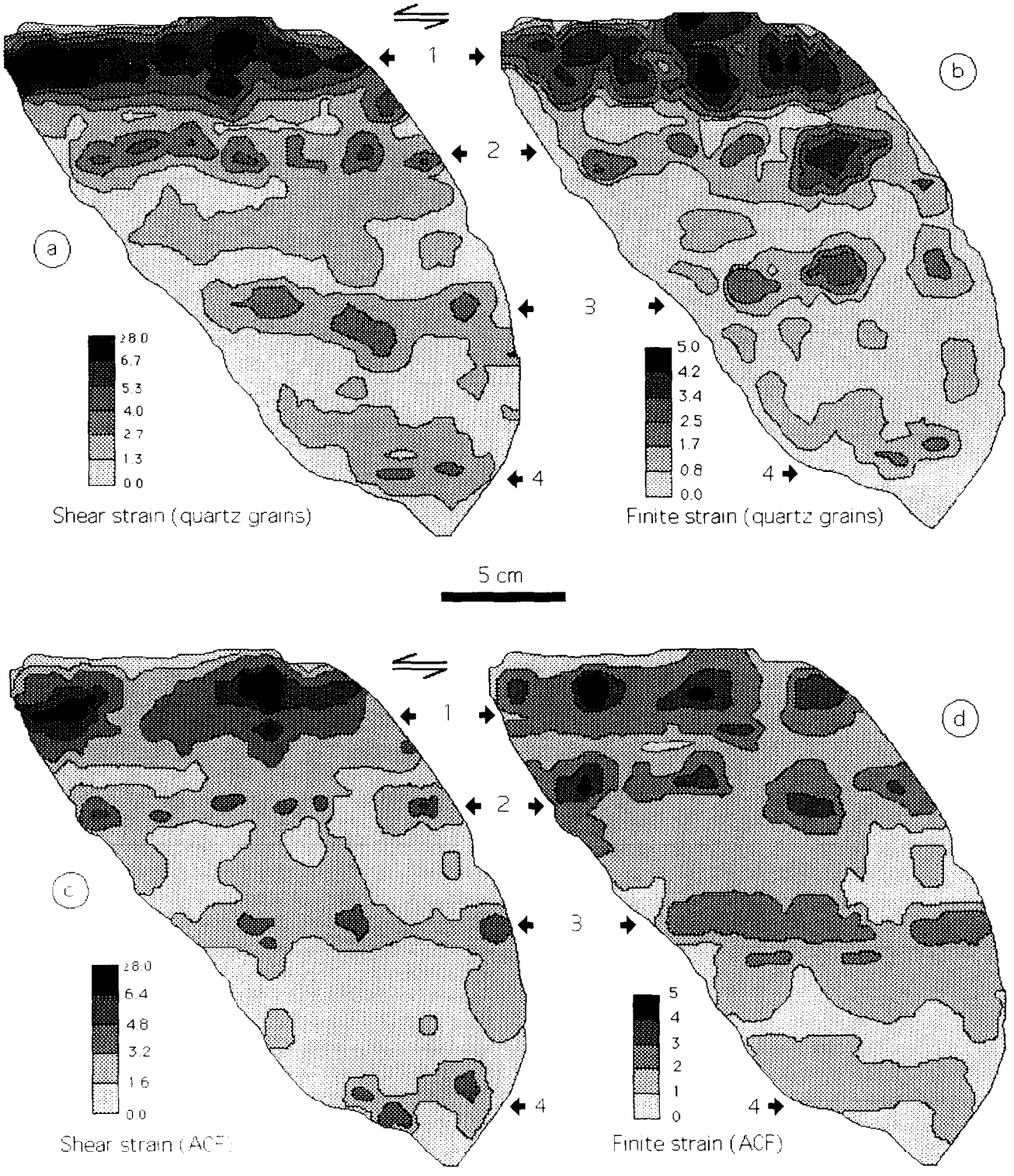

Fig. 3. Sample 1 strain distribution. (Arrows: zones of high strain magnitude.) (a) Shear strain determined from quartz grain orientation. Maximum of shear strain: $\gamma = 8$. Smooth surface contains 1013 strain data. See text for method. (b) Finite strain expressed as axial ratio of the strain ellipses estimated from deformed quartz grains; 1013 data for map drawing. [e_1/e_3: e_1, e_3: principal finite extensions of X and Z, respectively.] (c) Shear strain from the average orientation of autocorrelation function pattern. The initial rock section image is cut along a regular grid into 248 parts. (d) Finite strain expressed as the average ellipticity from the autocorrelation function central patterns (248 data for map drawing).

ing the strain distribution, which we will apply in the following section.

Results of strain analysis

The analysis of each quartz grain shape was applied on sample 2 and sample 3 in order to obtain shear strain maps (Figs. 4a & b, respectively). Strain distribution is not as clear as in sample 1 and is influenced by the shape of the sections studied having length much too large with respect to width, which produces edge effects in the map interpolation. Despite this problem, a band of high shear strain ($\gamma = 6.8$ for sample 2, Fig. 4a; $\gamma = 13$ for sample 3, Fig. 4b) is located close to the higher strained

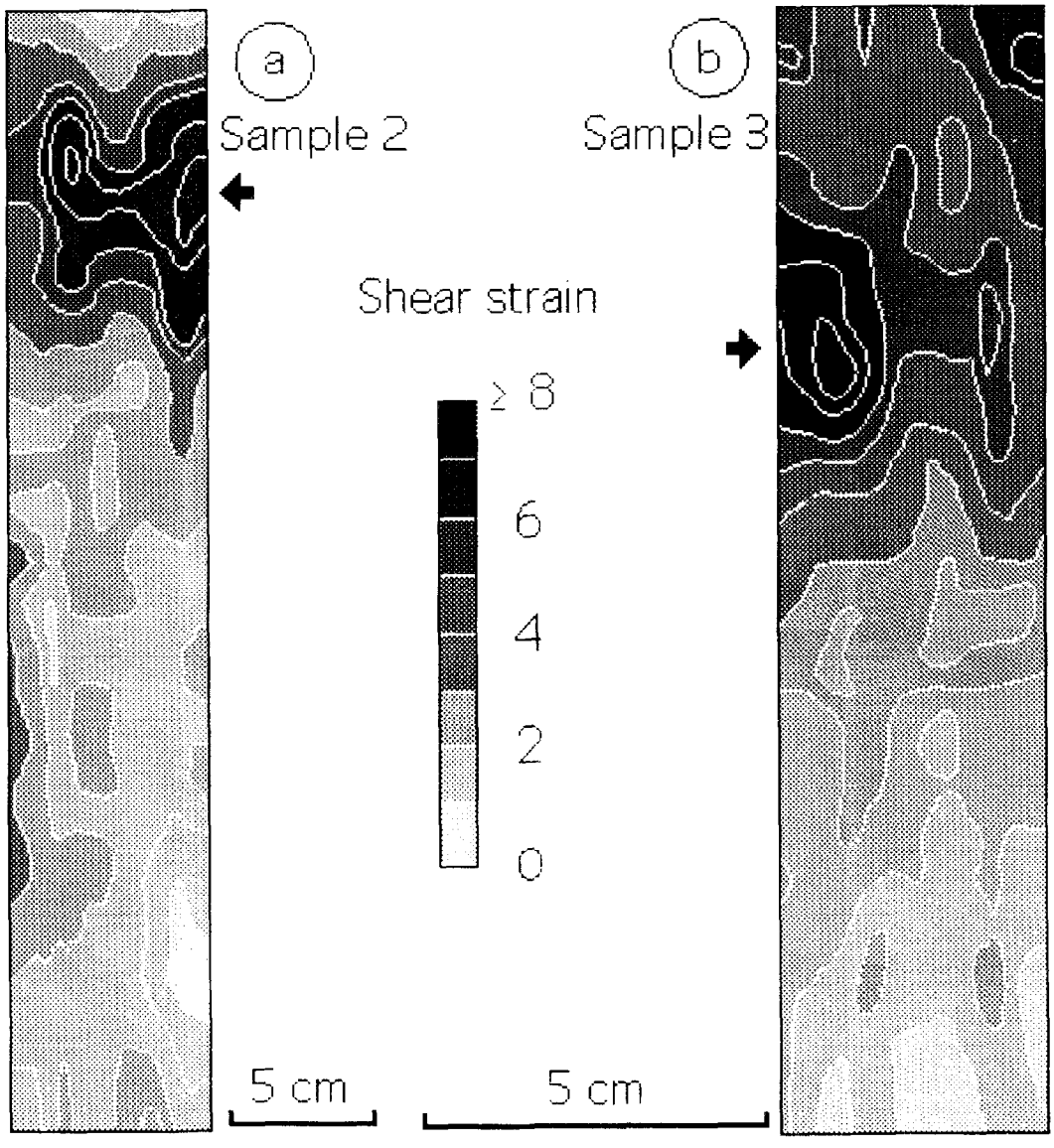

Fig. 4. Shear strain maps obtained by each quartz grain analysis. (a) Sample 2 map: photographs of the polish section are analysed. Maximum of shear strain: $\gamma = 7$. (b) Sample 3 map: this map is obtained from thin section analysis and corresponds to the upper part of the sample. Maximum of shear strain: $\gamma = 13$.

facies, at 6 cm from the top of the shear zone (sample 2) and 5 cm from that of sample 3. Otherwise, the gradient decreases without obvious alignment of high shear strain regions in the shear direction. Alignments perpendicular to the shear direction are identified as interpolation edge artefacts.

Strain profiles perpendicular to the shear direction (Fig. 5) are drawn from the strain maps. Data are put together on a synthetic single profile in order to analyse the major shear strain variations. We have calculated from the strain values the best fitting curve that corresponds to an exponential profile (Fig. 5). This exponential fit profile is considered as a *background* strain profile. It is compatible with the smoothed profile obtained by the technique using the angular deflection of the trace of passive strain markers (Ramsay 1980). Bands of strain localization on the maps correspond to peaks on profiles, with strain values ($\Delta\gamma \geq 2$–0.5) higher than the exponential profiles (Fig. 6). These peaks are a few centimetres wide, which is approximately 10 grain diameters.

FREQUENCY ANALYSIS

Fast Fourier transform analysis limits

Strain maps and profiles suggest, at first glance, a periodic distribution of strain. Two techniques may be applied on a discrete signal to analyse significant frequencies. The fast Fourier transform (FFT) is the easiest method to determine low frequencies (frequency number $\leq$ 1000). Significant periods of a signal are isolated peaks of high amplitude (the signal-to-noise ratio is taken to be greater than 10). The statistical analysis (Thomson 1982, Robert *et al.* 1987) may be applied to noisy, discrete signals to determine significant high frequencies (frequency number $\geq$ 1000) without artefacts

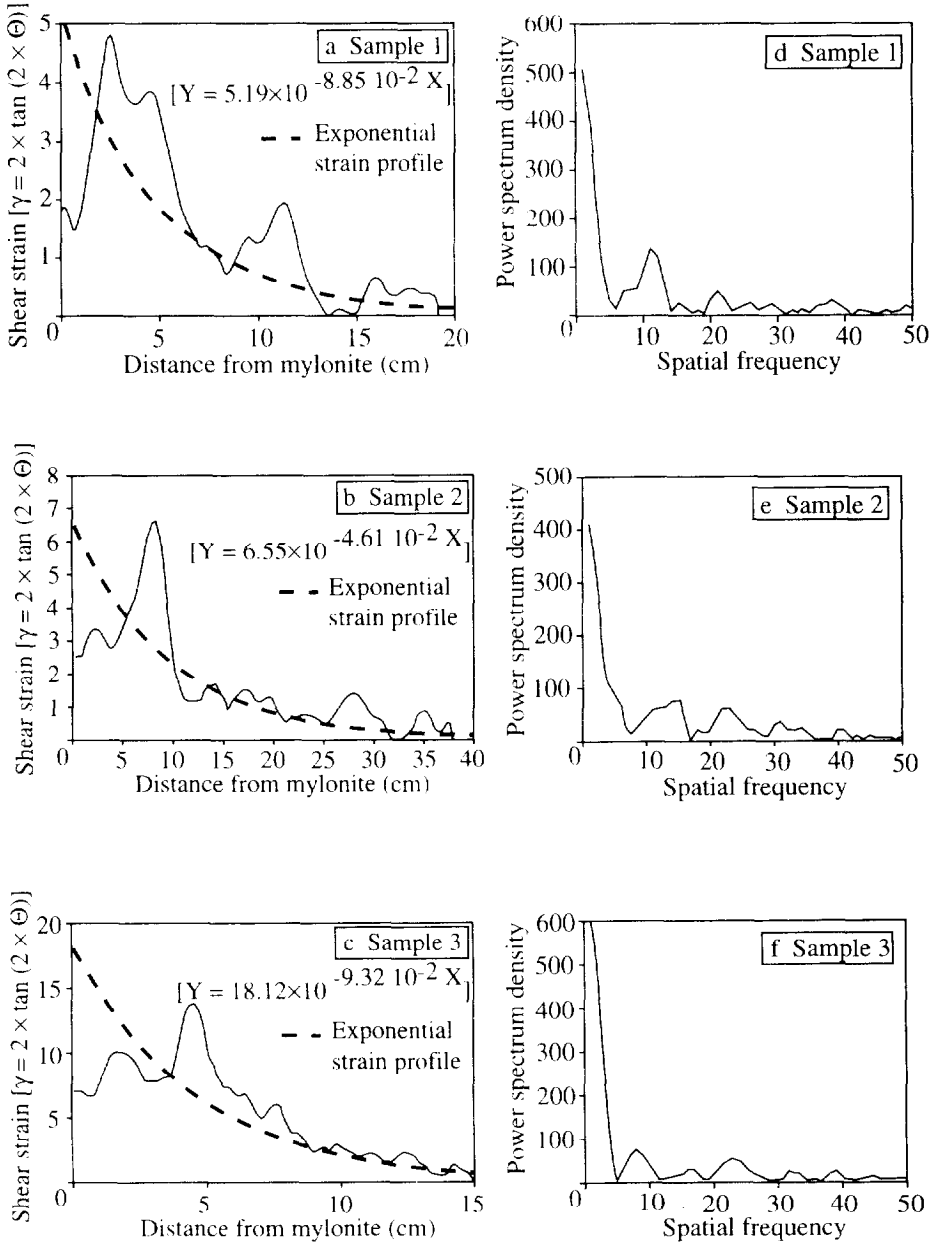

Fig. 5. Shear strain profiles orthogonal to the shear plane. Sample 1 (a) compared with the exponential strain profile obtained by Rey (1992). Sample 2 (b) compared with the equivalent smooth profile. Sample 3 (c) compared to profiles measured by Burg & Laurent (1978). Spatial frequency analysis obtained by the FFT technique for sample 1 (d), sample 2 (e) and sample 3 (f). The higher amplitude peak ($f = 1$) is related to the regular strain component and spatial periodicity is contained into smaller peaks ($1 < f \leq 40$).

due to sampling and spectral leakage (Park *et al.* 1987, Negi *et al.* 1990). In the spectra obtained from the three strain profiles, significant wavelengths have periods larger than 2.5 cm (i.e. frequency number ≤ 20). Therefore, profiles digitized with a regular sampling interval (d) have been analysed by the fast Fourier transform (FFT).

In general, the one-dimensional discrete Fourier transform for a discrete series of spatial measurements is given by the equation (Bergé *et al.* 1992):

$$X_k = \frac{1}{N} \sum_{j=0}^{N-1} xj \cdot \exp\,[-2\pi ijk/N].$$

where $i = \sqrt{-1}$; $k = 1, \ldots, n$; x_j, discrete spatial series; X_k, Fourier discrete series.

The frequency band given by the discrete FFT is limited by two different considerations related to initial sampling. First, digitizing the input strain profile with a sampling interval (d) introduces a distortion of the highest frequencies, known as 'aliasing'. However, the highest frequency can be restored by discretization and is called the Nyquist frequency. It is related to the sampling spatial interval (d) by the relation (Bergé *et al.* 1992):

$$f_{\text{Nyquist}} = \frac{1}{2d},$$

where f if the spatial frequency.

Second, the total length of the sample analysed limits the low frequency content of the spectra. It also provides the scale factor which allows the conversion of fre-

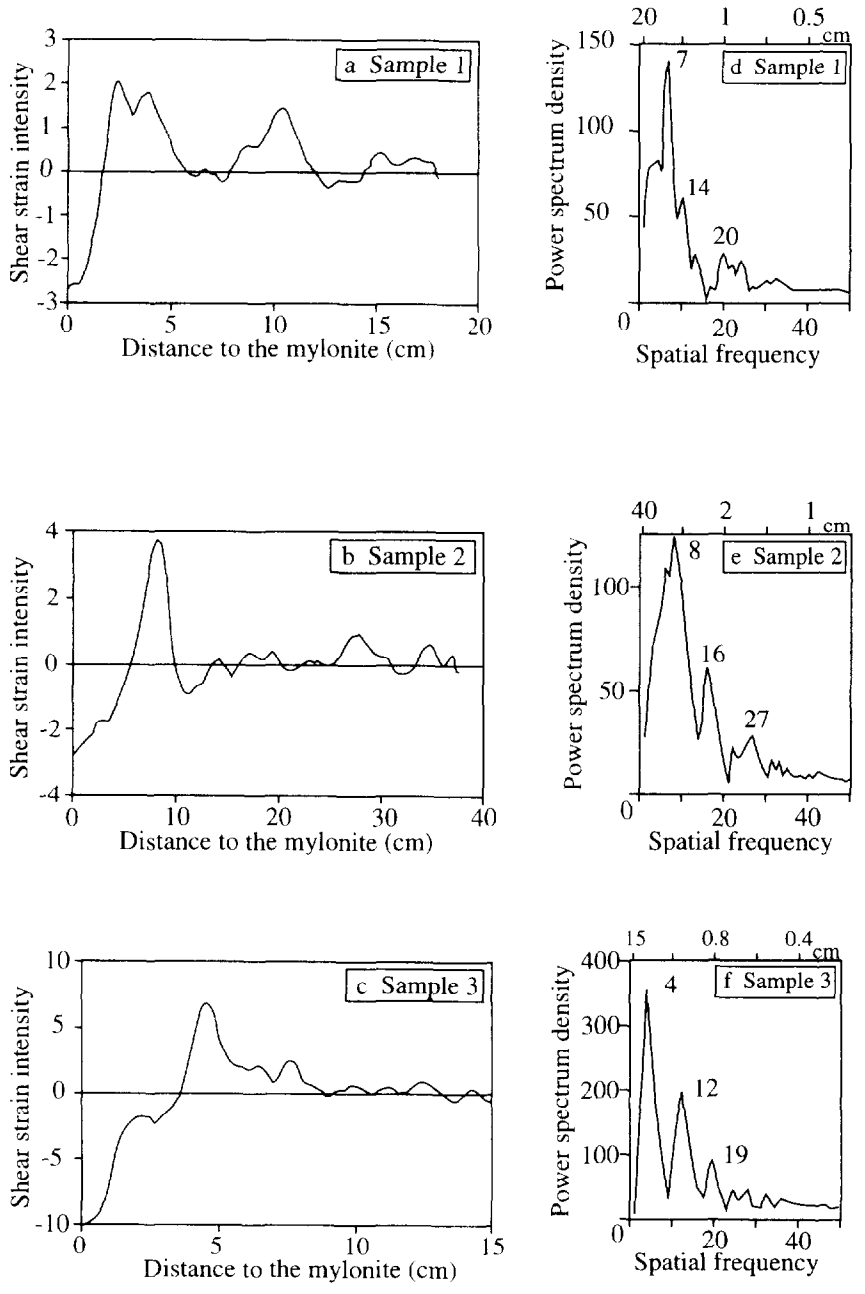

Fig. 6. Strain perturbations after subtraction of the exponential profile (corresponding to the first component). Sample 1 (a), sample 2 (b) and sample 3 (c). Corresponding frequency analysis of strain perturbations for sample 1 (d), sample 2 (e) and sample 3 (f). Significant frequencies are indicated on the curves.

quencies into wavelengths. Finally, we also took into account the wrap-around problem (Press *et al.* 1988) by computing the FFT spectrum on the profile and its symmetrized portion. Thus the function is by essence periodic in a mathematical way. Computing the spectrum on a symmetrized function does not introduce artefacts and reduces the high frequencies introduced when the FFT has to take into account the step difference in extreme values at the end of the profile (Gibbs phenomena).

Periodic distribution of shear strain

The computed spectra (Fig. 5) show that the highest contribution of strain is within the low frequency range (frequency number < 5). However, smaller peaks at medium frequencies ($5 \leq$ frequency number ≤ 20, Fig. 5) suggest that other components with distinct wavelengths are present. These secondary peaks reveal some harmonic component since the sample 1 spectrum presents peaks at frequency numbers 10, 20 and 38. Similarly, in the sample 2, secondary peaks are at 12, 24 and 36. In sample 3, peaks occur at fundamental frequency number 8, 16 and 24. The systematic presence of harmonics may indicate either a periodic distribution of strain superimposed on the large scale, or a low frequency decrease in strain from the central mylonite zone. Due to the large amplitude of the low frequency component in the spectrum, we extracted the medium frequency component from the total spectrum to better

Table 1. Main characteristics of the shear zones studied

Sample	Gsize (10^{-2} m)	T (°C)	int0	int1	int1/int0	b	w (10^{-2} m)	$\bar{\gamma}$
1	0.2	400 ± 50	1.9	4.8	2.5	8.85	5.0	1.49
2	0.5	350–450	2.6	6.6	2.5	4.61	2.8	1.52
3	0.15	≤350	7.1	13.7	1.9	9.32	3.8	4.49

Values of the grain size (Gsize), approximate temperature of deformation (T), strain intensity of the mylonite (int0), strain intensity of the first secondary peak (int1), ratio of the first intensity peak to the strain intensity of the mylonite (int1/int0), coefficient of the exponential decreasing curve of the far field approximation (b), computed wavelength of the periodic distribution of strain (w), average strain intensity ($\bar{\gamma}$).

determine the near field conditions which rule the strain localization.

The far field, which basically includes the low frequency component, has been fitted using an exponential curve of the type $\gamma = A \exp(-bx)$ to the strain profile (Figs. 5a–c). Then, the exponential fit computed from the strain values is removed from the strain profile before a new FFT analysis provides the near field spectrum. For each sample, the local field and its associated new spectrum are computed and displayed in Fig. 6. The near strain field corresponding to the three sample strain profiles (Figs. 6 a–c) shows a low strain region in the immediate vicinity of the mylonitic zone, and several intense shear bands at regular intervals. On the associated frequency spectra (Figs. 6d–f) two or three peaks reflect the periodic signature of the signal. On samples 2 and 3, the signal presents a maximum at frequency numbers 8, 16 and 27 and 4, 12 and 19, respectively. In the sample 1, two peaks are well defined at frequency numbers 7 and 20 and two smaller peaks occur at 11 and 14. Due to the low resolution of the total spectra on which the cut-off frequency has been set at 50, it is tempting to interpret the various peaks as harmonic frequencies (7, 14 and 21 in the sample 1; 8, 16 and 24 in sample 2 and 6, 12 and 18 in sample 3). When transposed into the spatial domain, the basal frequency associated to the first harmonics indicates a periodic occurrence of strain with a wavelength of 2.8 cm for sample 1, 5 cm for sample 2 and 3.8 cm for sample 3.

In order to make comparisons between the three shear zones, we have determined some values of interest regarding the central low strain region, such as its width (w) and the intensities of strain in the central mylonite (int(0)) and at the first shear band (int(1)). We also extract from the strain intensity profile the average strain value, as the integral of strain, normalized by the length of the profile (Ramsay 1980). All values are given in Table 1.

DISCUSSION

The central 'low strain' intensity area

At the grain scale of resolution, shear is localized on the three samples examined in discrete shear bands parallel to each other and to the most deformed mylonite zone. These bands are independently recorded by all θ, Rf and ACF methods applied to achieve a quantitative analysis (Figs. 3a–d).

Paradoxically, the very high strain of the mylonites is not detected within the three mylonite zones. Instead, centres of the mylonites appear as bands of small strain values, although the mylonites present extremely elongated quartz grains sub-parallel to the shear direction (C–S angle ≤ 5°). Strain analysis methods based on grain shapes and orientations appear therefore not appropriate to measure shear strain on the intensely deformed facies ($\gamma \geq 10$). This may result from a change in mechanism of quartz deformation (i.e. form ductile to super-plastic) below a critically small grain size.

We have tested the effect of the strain intensity in the centre of the mylonite (int(0)) and at the first secondary shear band (int(1)). The ratio int(1)/int(0) is large, ranging from 1.9 to 2.5 for our samples. These large ratios are significant and cannot be attributed to errors in the determination of the strain map values. On the strain intensity profiles, the width of the low intensity strain zone varies as a function of the strain registered in the first secondary zone (int(1)). The lower the intensity of the secondary strain zone, the wider the low intensity zone. In order to get a better calibration, the average strain has been computed by integrating the strain over a finite width and by computing the strain by length unit. Both sample 1 and 2 yield similar strain values ($\bar{\gamma} = 1.48$ and 1.52, respectively) whereas sample 3 is more highly strained ($\bar{\gamma} = 4.5$). This result corroborates the observation of a pronounced alignment of the shear bands close to the mylonite in sample 3. In the other samples of equal strain intensity, the size of the low strain zone widens with the grain size.

The low frequencies component of the spectrum

Several authors have indicated that a total shear value (S) cannot be obtained by the single ratio of the amplitude of displacement to the width of the displaced zone, but only by the integration of the displacement (Ramsay 1980):

$$S = \int_0^x \gamma dx.$$

It has been suggested that strain is distributed exponentially in the shear gradient. In our samples, shear

strain (γ) along the profile (x) is approximated by a decreasing exponential function of equation type:

$$\gamma = A \exp(-bx)$$

in which A and b are fitted coefficients. Examining their values for each samples, we see that the power coefficient (b) increases with grain size (Table 1) and the constant coefficient (A) weakly correlates to the average strain ($\bar{\gamma}$). But, the small number of samples precludes any large scale interpretation of these coefficients.

The medium frequencies component of the spectrum

To investigate the medium frequencies component, we filtered the strain profile by removing the low frequencies component. Filtering is a well known process in potential field methods to separate the far field effect (low frequencies) from the near field effect (medium frequencies). The resulting data are then analysed by a FFT process and peaks appear in the new frequencies spectrum (Fig. 6). The filter process emphasizes the medium part of the spectrum and does not add significant artefacts. Peaks in the strain profiles (Fig. 5) have an approximate wavelength corresponding to that computed from the FFT analysis. In addition, the three peaks of the frequency spectrum interpreted as harmonic frequencies reinforce the interpretation of a periodic distribution of strain along the profile.

The distribution of localized high strain bands is very different from the grain size, so it cannot be introduced by the sampling interval. In all samples the computed wavelength of the periodic distribution of strain ranges from 2.8 to 5 cm whereas the grain size is 0.15–0.5 cm. In addition, the sampling rate is about 10 pixel per grain. Therefore, the shear band distribution and its associated wavelength does not result from sampling artefacts. In a similar way, the strain intensity profiles present several peaks, which allows the FFT process to operate. At least three peaks are quite distinct on the three strain profiles (Fig. 5). So we may conclude that the periodic distribution exists, at least at the sample scale, and does not result from artefacts in the FFT analysis. However, once the existence of discrete parallel shear bands are considered, explanations must focus on mechanisms which determines such periodicity. One consists in having a real periodicity in shear bands. This exists in cold experiments or can develop in Luders bands in hot-rolled shear (Harren *et al.* 1988, Hansen 1990). One alternative explanation relates to a periodic distribution of weaker mineral which concentrates deformation. However, we examined the distribution of quartz aggregates (Fig. 2a) and found that it does not show a heterogeneous distribution.

CONCLUSION

Strain analysis of three minor shear zones suggests heterogeneous strain patterns on XZ maps. The maps have a detailed resolution due to the point-to-point analysis obtained from quartz distribution. From this study, the following points may be underlined:

(1) Shear strain decreases exponentially from the mylonite to the granite protolith.

(2) Finite strain (R_S) and shear strain (γ) are localized into discrete bands sub-parallel to the shear plane of continuous shear zones.

(3) Localization bands correspond to domains of numerous and merging shear planes.

(4) The bulk distribution of the shear bands is periodic. Perturbation induced on regular strain profiles correspond to two or three distinct wavelengths.

(5) The intensely sheared, central part of ductile shear zones is characterized by a change in deformation mechanism or may be related to other reaction processes involving quartz (mass transfer of silica, for example).

At that scale of observation, the strain localization may be due to physical parameters such as grain size (Kronenberg & Tullis 1984, Dutruge *et al.* 1993) mineral strength and rheology or viscosity contrast (Treagus & Sokoutis 1992). We have to make further observations to analyse the influence of these physical parameters on strain localization.

Acknowledgements—This work has been partially financed by the INSU-CNRS (ATP-92 EC 05). We thank M. Casey, M. Jessell, D. Mamprice and R. Weijermars for improving a first manuscript and D. Marquer for his helpful interest.

REFERENCES

Bak, J., Sorensen, K., Grocott, J., Korstgard, J. A., Nash D. & Watterson J. 1975. Tectonic implications of Precambrian shear belts in western Greenland. *Nature* **254**, 566–569.

Berge, P., Pomeau, Y. & Vidal, C. 1992. *L'ordre dans le chaos—Vers une approche déterministe de la turbulence*. Hermann Ed., Paris.

Berthé, D., Choukroune, P. & Jegouzo, P. 1979. Orthogneiss, mylonite and non-coaxial deformation of granites: the example of the south armorican shear zone. *J. Struct. Geol.* **1**, 31–42.

Burg, J. P. & Laurent, P. 1978. Strain analysis of a shear-zone in a granodiorite. *Tectonophysics* **47**, 15–42.

Burg, J. P. & Teyssier, C. 1983. Contribution à l'étude tectonique et microtectonique des séries cristallophylliennes du Rouergue oriental: la déformation des laccolites syntectoniques, type Pinet. *Géologie de la France* **1–2**, 3–30.

Burg, J. P. & Wilson, C. J. L. 1987. Deformation of two phase systems with contrasting rheologies. *Tectonophysics* **135**, 199–205.

Choukroune, P., Gapais, D. & Matte, P. 1983. Tectonique hercynienne et déformation cisaillante: la faille ductile sénestre de la Marche (Massif Central français). *C. r. Acad. Sci., Paris, Sér.* II **296**, 859–862.

Dunnet D. 1969. A technique of finite strain analysis using elliptical particles. *Tectonophysics* **7**, 117–136.

Duthou, J. L., Cantagrel, J. M., Didier, J. & Vialette, Y. 1984. Paleozoic granitoids from the French Massif Central: age and origin studied by ^{87}Rb–^{87}Sr system. *Phys. Earth & Planet. Interiors* **35**, 131–144.

Dutruge, G., Chery, J. & Hurtrez, J. E. 1993. Une approche numérique des effets de la taille de grain sur la localisation de la déformation ductile. *C. r. Acad. Sci., Paris* **317**(2), 195–201.

Etsley, E. A. 1988. Normalized center-to-center strain analysis of packed aggregates. *J. Struct. Geol.* **10**, 201–209.

Escher, A., Escher, J. C. & Watterson, J. 1975. Reorientation of the Kangâmiut Dyke Swarm, West Greenland. *Can. J. Earth Sci.* **12**, 158–173.

Flinn, D. 1962. On folding during three dimensional progressive deformation. *Q. J. geol. Soc. Lond.* **118**, 385–433.

Grocott, J. & Watterson, J. 1980. Strain profile of a boundary within a large ductile shear zone. *J. Struct. Geol.* **2**, 111–117.

Hansen, N. 1990. Cold deformation microstructures. *Mater. Sci. Technol.* **6**, 1039–1047.

Harren, S. V., Deve, H. E. & Asaro, R. J. 1988. Shear band formation in plane strain compression. *Acta metall.* **36**, 2435–2480.

Kronenberg, A. K. & Tullis, J. 1984. Flow strengths of quartz aggregates: Grain size and pressure effects due to hydrolytic weakening. *J. geophys. Res.* **89**, 4281–4297.

Lisle, R. J. 1977. Estimation of the tectonic strain ratio from the mean shape of deformed elliptical markers. *Geologie Mijnb.* **56**, 140–144.

Negi, J. G., Tiwari, R. K. & Rao, K. N. N. 1990. 'Clean' spectral analysis of long-term sea-level changes. *Terra Nova*, **2**, 138–141.

Panozzo-Heilbronner, R. 1992. The autocorrelation function: an image processing tool for fabric analysis. *Tectonophysics* **212**, 351–370.

Park, J., Lindberg, C. R. & Vernon III, F. L. 1987. Multitaper spectral analysis of high-frequency seismograms. *J. geophys. Res.* **92**, 12,675–12,684.

Press, W. H., Flannery, B. P., Teukolsky, S. A. & Vetterling, W. T. 1988. *Numerical Recipies—The Art of Scientific Computing*. Cambridge University Press, Cambridge.

Ramsay, J. G. 1980. Shear zone geometry: a review. *J. Struct. Geol.* **2**, 83–99.

Ramsay, J. G. & Allison, I. 1979. Structural analysis of shear zones in an Alpinised Hercynian Granite. *Schweiz. miner. Petrogr. Mitt.* **59**, 251–279.

Ramsay, J. G. & Graham, R. H. 1970. Strain variation in shear belts. *Can. J. Earth Sci.* **7**, 786–813.

Ramsay, J. G. & Huber, M. I. 1983. *The Techniques of Modern Structural Geology—Vol. 1: Strain Analysis*. Academic Press, London.

Rey, P. 1992. Effondrement de la chaine Varisque dans les Vosges et fabrique sismique de la croûte continentale. Doctorat, Université Grenoble I, France.

Robert, D. J., Lehar, J. & Dreher, J. W. 1987. Time series analysis with clean, derivation of spectra. *Astron. J.* **93**, 968–989.

Thomson, D. J. 1982. Spectrum estimation and harmonic analysis. *IEEE Proc.* **70**, 1055–1096.

Treagus, S. H. 1981. A simple-shear construction from Thomson & Tait (1867). *J. Struct. Geol.* **3**, 291–293.

Treagus, S. H. & Sokoutis, D. 1992. Laboratory modelling of strain variation across rheological boundaries. *J. Struct. Geol.* **14**, 405–424.

Tullis, T. E., Horowitz, F. G. & Tullis, J. 1991. Flow laws of polyphase aggregates from end member flow laws. *J. geophys. Res.* **96**, 8081–8096.

Weijermars, R. 1987. The construction of shear strain profiles across brittle–ductile shears. *Annu. Geophys.* **5B**, 201–210.